Temporal Firing Patterns of Purkinje Cells in the Cerebellar Ventral Paraflocculus During Ocular Following Responses in Monkeys I. Simple Spikes

HIROAKI GOMI,[1,4] MUNETAKA SHIDARA,[2,4] AYA TAKEMURA,[2,4] YUKA INOUE,[2,4] KENJI KAWANO,[2,4] AND MITSUO KAWATO[3]

[1]*NTT Basic Research Laboratories, Nippon Telegraph and Telephone Corporation, Kanagawa 243-0198;* [2]*Neuroscience Section, Electrotechnical Laboratory, Ibaragi 305-8568;* [3]*ATR Human Information Processing Research Laboratories, Kyoto 619-0228; and* [4]*JST-CREST, Ibaraki 305-8568, Japan*

Gomi, Hiroaki, Munetaka Shidara, Aya Takemura, Yuka Inoue, Kenji Kawano, and Mitsuo Kawato. Temporal firing patterns of Purkinje cells in the cerebellar ventral paraflocculus during ocular following responses in monkeys. I. Simple spikes. *J. Neurophysiol.* 80: 818–831, 1998. The simple-spike firing frequency of 30 Purkinje cells (P cells) in the ventral paraflocculus (VPFL) of alert monkeys was studied in relation to vertical slow eye movements, termed ocular following response (OFR), induced by large-field visual motions of different velocities and durations. To quantitatively analyze the relationship between eye movement and firing frequency, an inverse dynamics representation of the eye movement was used for reconstructing the temporal waveform of firing. Coefficients of eye-acceleration, velocity, and position, bias, and time lag between firing and eye movement were estimated by least-square error method. In the regression analyses for each stimulus condition, 86% (146/170) of the well-modulated temporal firing patterns taken from those 30 P cells were reconstructed successfully from eye movement. The model with acceleration, velocity, and position terms, which we used, was shown as the best among several potential models by Cp statistics, consistent with *t*-test of significance of each term. Reliable coefficients were obtained from 75% (109/146) of the well-reconstructed firing patterns of 28 cells among 30. The estimated coefficients were larger (statistically significant) for slow stimuli than for fast stimuli, suggesting changes in sensitivities under different conditions. However, firing patterns of each cell under several different conditions were frequently well reconstructed by an inverse dynamics representation with a single set of coefficients (13 cells among 21). This indicates that the relationships between P cell firing and OFR are roughly linear in those stimulus ranges. The estimated coefficients for acceleration and velocity suggested that the VPFL P cells properly encode the dynamic components of the motor command during vertical OFR. As for the positional component, however, these P cells are correlated with eye movement in the opposite direction. In the regression analysis without positional component, remarkable differences between observed and reconstructed firing patterns were noted especially in the initial phase of the movements, indicating that the negative positional component was not negligible during OFR. Thus we conclude that, during OFR, the VPFL P cells cannot provide the necessary final motor command, and other brain regions, downstream neural structures, or other types of P cells must provide lacking position-dependent motor commands. This finding about the negative correlation with the position is in the opposite sign with previous studies obtained from the fixation and the smooth pursuit movement. From these comparisons, how the VPFL contributes to a part of the final motor command or how other brain regions complement the VPFL is suggested to be different for early and late phases of the movements.

INTRODUCTION

Correlational study of neural firing has been one of the most successful methods used for elucidating how particular brain regions contribute to motor control, along with lesion study, electrical stimulation, and physiological and anatomic studies of the neural networks involved. Especially after the pioneering study of Evarts (1968), correlation studies were major techniques used in awake animals to elucidate which aspect of the movement is best correlated with the neural firings of a specific brain region and furthermore what information the neural firing encodes. Evarts and his colleagues (Evarts 1968; Evarts and Tanji 1976) examined correlations between the firing of motor cortex neurons and the position and force of movements and concluded that force is represented. By using the spike trigger averaging method, Cheney and Fetz (1980) identified a class of neuron in the primary motor cortex that directly innervates the spinal motor neurons. Georgopoulos and his colleagues (Georgopoulos et al. 1982, 1986; Kalaska et al. 1983) examined correlations between multijoint arm reaching movements and neural firings of several cerebral cortical areas, such as the primary motor cortex, premotor cortex, and area 5, and found that the firings are correlated with movement directions. These previous studies brought us very important insights into how neural firings in the brain are correlated with observed movements. However, we feel that these past methodologies have some limitations in regard to the following two points. First, in most cases temporally averaged firing frequencies were examined and the instantaneous firing frequency was not explicitly treated. Second, we cannot directly examine how the dynamic motor commands of the motor neurons are generated in the brain. In other words, we cannot examine which portion of the dynamic motor command is generated by a particular brain region.

To overcome these two shortcomings, we have proposed a method useful for correlation studies, the inverse dynamics approach (Kawano et al. 1996; Shidara et al. 1993). Here, the temporal firing patterns are fitted by kinetic information

containing a motor apparatus. From best-fit parameter values, we can examine which portion of the final motor command is represented by the temporal pattern of the instantaneous firing frequency of neurons in some brain region under consideration. If the firing patterns can be well reconstructed by an inverse dynamics representation, we can understand not only what information is encoded in that neural activity but also which portion of the motor command is still lacking. This might allow us to suggest what downstream neural structure and what parallel pathways are necessary to calculate the final motor commands. Additionally, by comparing coefficients, this analysis could reveal how the brain region is involved in different movements and different phases of the same movement. Furthermore, this method could be a general technique that can examine the correlation of neural firing with the final motor commands for many biologically controlled objects such as a multijoint arm that involve nonlinear dynamics, because the inverse dynamics equation can be represented as a weighted summation of some nonlinear and linear terms of acceleration, velocity, and position of the movement trajectory (Craig 1989).

Although a forward model has been used to analyze the instantaneous firing frequency associated with some movements in previous studies (Berthier et al. 1991; Krauzlis and Lisberger 1994), it suffers from the fundamental difficulty that the movement cannot be predicted from only one brain region's activity if other brain regions also contribute to some part of the final motor command. In this sense, the inverse dynamics approach is a more versatile tool for correlation study of neural activities.

Neural activities associated with ocular following responses (OFR) (Miles et al. 1986) induced by movements of a large-field visual scene were recorded in several brain regions: the medial superior temporal area (MST) (Kawano et al. 1994), the dorsolateral pontine nucleus (DLPN) (Kawano et al. 1992), and the ventral paraflocculus (VPFL) (Shidara and Kawano 1993) of the cerebellum. From these studies, it was inferred that the neural firings in MST and DLPN encode the visual input signals and that the Purkinje cells (P cells) in VPFL send the eye driving signals. The purpose of the present study is to reveal the role of the cerebellum in controlling OFR by examining neural firing frequencies from the viewpoint of dynamic motor control.

In spite of the preceding attractive points of the inverse dynamics analysis, our previous reports of this study (Kawano et al. 1996; Shidara et al. 1993) were limited to analyzing only well-modulated firing patterns averaged over many trials (23 cells, only either 80 or 160°/s stimulus velocity in the preferred direction in the local analysis, with data shown for only 1 cell for multiple stimulus velocities only in the preferred direction with fixed stimulus duration). This limitation was caused by the insufficient method used for fitting evaluation. Thus we could not analyze firing patterns under low speed stimuli and firing patterns averaged from smaller numbers of trials, resulting in difficulties in examining in a sufficient number of cells the condition-dependent changes in the relationship between P cell firing patterns and eye movements. Additionally, even in the global analysis, it was difficult to correctly evaluate the fitness of the model with only a single measure of the fitness.

In this paper, by using multiple statistical methods that can objectively examine goodness-of-fit of the model and parameter reliability, we have analyzed a larger volume of data (232 firing patterns) measured from 30 P cells of three monkeys for a much wider variety of visual stimulus conditions (i.e., 5 stimulus speeds in preferred direction, 5 stimulus speeds in antipreferred direction, and 6 stimulus durations). With this much larger data set, we can fully discuss the generality and applicability of the inverse dynamics analysis, and the physiological insights obtained from it.

METHODS

Experimental setup

The experimental conditions are the same as in Shidara and Kawano (1993) and Kawano, Shidara, and Yamane (1992). Briefly, monkeys (*Macaca fuscata*) were pretrained to fixate a small target spot to obtain a fluid reward. Under pentobarbital sodium (Nembutal) anesthesia and aseptic conditions, each monkey was implanted with a cylinder for microelectrode recording in VPFL (Shidara and Kawano 1993) and fitted with a head holder that allowed the head to be fixed in the standard stereotaxic position during the experiment. Scleral search coils were implanted to measure eye movements (Judge et al. 1980).

The monkeys faced a translucent tangent screen ($85 \times 85°$ at a distance of 235 mm), on which moving random-dot patterns were back-projected via a galvanometer mirror system. The visual stimulus started to move at 10–160°/s in a preferred direction or an antipreferred direction 50–250 ms after the end of a centering saccade. Preferred direction here denotes the direction among eight directions (up, down, left, right, and intermediate directions between these 4 directions) in which each P cell was activated most vigorously (Shidara and Kawano 1993). Each visual stimulus ramp lasted 250 ms in the stimulus speed change conditions. Note that, after ~250 ms, induced smooth eye movement frequently is interrupted by a saccade. In the stimulus duration change condition, the stimulus lasted 10–160 ms. OFR induced by the motion of the whole field retinal image began with short latency (~50 ms) compared with that in smooth pursuit eye movements.

During OFR, the mirror velocity and the horizontal and vertical components of eye position and eye velocity [measured with the search coils and filtered with a 6-pole analog Bessel filter (100 Hz)], were recorded at 500 Hz. The speed of the random dot pattern on the screen was in proportion to the mirror velocity. The single P cell simple spike activity of VPFL was discriminated with a time-amplitude window discriminator and simultaneously recorded at 1,000 Hz.

Data preparation

To analyze the relation between the VPFL P cell firing frequency and eye movement, the P cell firing frequency and eye movement during many trials (14–317 trials, average ± SD = 95.5 ± 36.9) under the same stimulus conditions were ensemble averaged for each P cell after excluding the trials with saccadic intrusion. The responses were aligned with the stimulus onset (*time 0*), and the eye acceleration profiles were obtained by digital differentiation of eye velocity profiles after the averaging. To align the filtering delays, the ensemble average firing pattern (i.e., firing frequency temporal pattern) was low-pass filtered with a 6-pole Bessel digital filter with the same cutoff frequency (100 Hz) as that of the analog filter for the eye movements. Shidara and Kawano (1993) showed that in OFR the preferred direction of the visual stimulus motion was either ipsiversive or downward for the VPFL P cells. In this

TABLE 1. *Stimulus conditions for each cell*

Unit Name	Preferred Speed	Antipreferred Speed	Duration
ed16a	All		All
edg0b	All		
edg1e	80		
edg2b	All		
edg3f	10, 20, 40, 80		
edg4a	All		
edg5c	All		
edg7b	All		
gc10a			All
gc15d			10, 20
kc38a	80		
kc38b	80	−80	
kc38c	80	−80	
kc40b	80	−80	
kc42a	All	All	
kc45a	80	−80	
kcg1c	All	All	
kcg2c	All	All	
kcg3d	All	All	
kcg4a	All	All	
kcg4b	All	All	
kcg4c	All	All	
kcg6g	All	All	
kcg7a	All	All	
kcg7b	All	All	All
kcg8c	All	All	
kcg9d	All	All	
kcgab	All	All	All
kcgbc	All	All	All
kcgcc	All	All	All
No. of cells	28	19	7
No. of data sets	115	79	38

Stimulus conditions for each cell. ''All'' in the column denotes the existence of data sets in all stimulus conditions as follows. In the preferred direction stimulus condition, the random dot stimulus patterns were applied at five speeds: 10, 20, 40, 80, and 160°/s. In the antipreferred direction stimulus condition, the stimulus speeds were changed to −10, −20, −40, −80, and −160°/s. In the duration change condition, stimulus patterns were eliminated by a mechanical shutter, 10, 20, 40, 60, 80, and 160 ms after the onset of stimulus movements of 80°/s. Numbers in the columns denote the condition parameter; that is, speed (unit, deg/s) or duration (units, ms) for neurons for which all stimulus patterns were not applied in the experiment.

paper, we focus only on the P cells the preferred directions of which were downward because of the small number of data sets in the horizontal direction. Table 1 summarizes the experimental conditions for 232 data sets from 30 P cells. Note that the number of applied stimulus conditions was different for different cells. During the experiment, we could not know whether the model predicted firing patterns well or not, so there was no way to intentionally change the number of stimulus conditions for good- and ill-fitting cells.

Figure 1 shows typical simple-spike activity of a P cell in the left VPFL together with eye angular acceleration, velocity, and position during OFR evoked by a 40°/s downward test ramp movement of a large-field random dot pattern (ensemble average of 194 trials). The firing frequency of this neuron suddenly increased 51 ms after the onset of stimulus motion. In the data shown, the eyes began moving several milliseconds after the onset of the neural responses.

Analysis method

P CELL FIRING RECONSTRUCTION. To analyze the relation between eye movement and neural activity, we used an inverse-dynamics representation that could reconstruct temporal patterns of the ensemble average firing frequencies of P cells. The representation is based on the following equation

$$\hat{f}(t-\delta) = M\ddot{\theta}(t) + B\dot{\theta}(t) + K\theta(t) + f_{\text{bias}} \quad (1)$$

where, $\hat{f}(t)$, $\ddot{\theta}(t)$, $\dot{\theta}(t)$, $\theta(t)$, δ, and f_{bias} are, respectively, the reconstructed firing frequency at time t; the eye acceleration, velocity, and position at time t; the time lag between the firing frequency and the movement; and the bias term. We assume the same delay for each component because of the following two reasons. One is that all components are mixed in the output (firing pattern) of the VPFL that is sent to eye motoneurons with little time lag. Different delays for different components are therefore unlikely. The other is to avoid the increase of the degree of freedom in the model. Note that the bias term does not directly correspond to the spontaneous firing level because it could contain a positional bias term. The four coefficients M, B, K, and f_{bias} and the time lag δ were estimated so as to minimize the squared error between the observed and the reconstructed firing frequencies (i.e., $f(t)$ and $\hat{f}(t)$, respectively) shown in *Eq. 2*

$$E(\delta, M, B, K, f_{\text{bias}}) = \sum_t [\hat{f}(t) - f(t)]^2 \quad (2)$$

A linear regression method was applied to estimate M, B, K, and f_{bias} at a particular δ while the best δ was globally and exhaustively searched over a range. Thus there is no danger that any global optimal solution was missed. The plausible transmission time from a P cell firing to an eye-ball movement is estimated to be ~9 ms

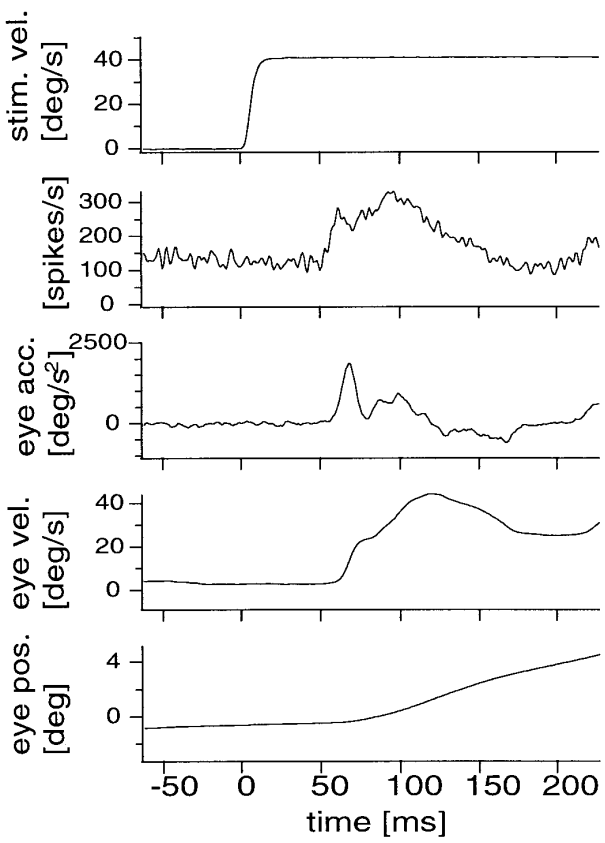

FIG. 1. Ensemble averaged patterns of 194 trials under the same stimulus condition (preferred direction stimulus 40 deg/s). From *top* to *bottom*: visual stimulus velocity, firing frequency of a single Purkinje cell (P cell), eye angular acceleration, eye angular velocity, and eye angular position.

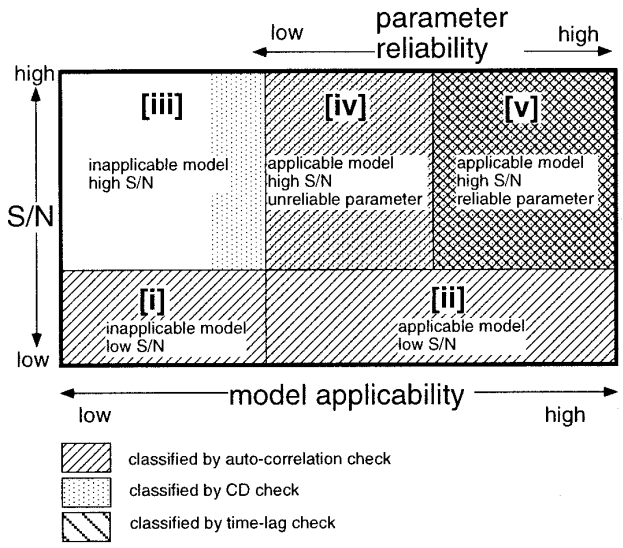

FIG. 2. Five data groups classified from the viewpoint of a regression analysis and a parameter estimation. Three requisites should be satisfied for reliable parameter estimation: applicable model, high S:N, and low correlation among regressor data. If the regression model is inapplicable, the data belongs to [*iii*]. If the neuron is not modulated sufficiently, the data belongs to [*i*] or [*ii*]. Even if the model is applicable and S:N is sufficiently high, the data should be classified into [*iv*] when the correlation among regressor data is high.

(Lisberger 1988) or 8.6–10.9 ms (Shidara and Kawano 1993), thus the search range for δ was limited from -20 to 20 ms.

MODELING CHECK FOR RELIABLE PARAMETER ESTIMATION. The squared error criterion can be used to evaluate the goodness-of-fit of the preceding model but is insufficient for determining whether reliable parameters are obtained. To examine the reliability of the estimated parameters, we should check the applicability of the model, signal to noise (S:N) ratio, and correlations between explanatory variables in the right-hand side of *Eq. 1*. For example, even if the fitness criterion, the coefficient of determination (defined in APPENDIX A), is highly scored, some trends in the residual errors may indicate that the applied model is inappropriate for the data, hence, the estimated parameters would be unreliable. In addition, high correlations among acceleration, velocity, and position signals degrade the estimation reliability in a multiple-parameter regression even though the firing pattern can be reconstructed well. Considering these factors, the data can be classified into five categories as shown in Fig. 2. Note that, to examine the relation between neural firing patterns and eye movements without failure caused by regression ambiguities, we should not rely on all parameters estimated. Rather we should focus only on the reliable parameters obtained from the data belonging to category [*v*] in Fig. 2. We applied the following three statistical methods to classify the data into the categories shown in Fig. 2. First, to categorize the data belonging to [*iii*], for which the model was inapplicable, the residual error of the modeling was analyzed by the autocorrelation method. If most of data sets are classified in [*iii*], the model is insufficient to characterize the activities of VPFL during OFR. Second, to classify the data that had sufficient S:N ratio and fitness to the model, a statistical index, the coefficient of determination, was evaluated as in the previous study (Shidara et al. 1993). Combining these two methods, we can discriminate the data belonging to *group* [*i*] or [*ii*], the S:N ratios of which are insufficient for parameter estimation, and the data belonging to *group* [*iv*] or [*v*] for which the applied model is applicable and S:N ratio is sufficient. Third, to examine the parameter reliability, we checked the estimation sensitivities of time lags and confidence intervals of all other parameters. Note that the confidence intervals take into account possible correlations between the explanatory variables (acceleration, velocity, and position) and estimation errors of one parameter caused by errors by the other parameters. In addition to these three methods, model applicabilities were evaluated by Cp statistics and *t*-test. The details of these statistical methods are explained in the appendices.

RESULTS

To examine the relation between P cell activity and eye movement under single and multiple stimulus conditions separately, local (single stimulus condition) and global (multiple stimulus conditions) fittings of P cell firing by *Eq. 1* were carried out.

Local condition analysis

RECONSTRUCTION OF P CELL FIRING FREQUENCY. The local fitting will describe the local characteristics, and by comparing local fittings for different stimulus conditions, we can examine how firing characteristics depend on stimulus dimensions. Figure 3*A* shows an observed firing frequency pattern (dotted line, the same data as in Fig. 1) and a reconstructed P cell firing frequency pattern (solid line) derived from the eye movement with estimated coefficients, M [0.0621 (spikes/s)/(deg/s^2)], B [4.6641 (spikes/s)/(deg/s)], K [-26.5471 (spikes/s)/(deg/s)], and a time lag, δ (7 ms). The coefficient of determination (CD) was 0.93, indicating that the simple linear inverse-dynamics represen-

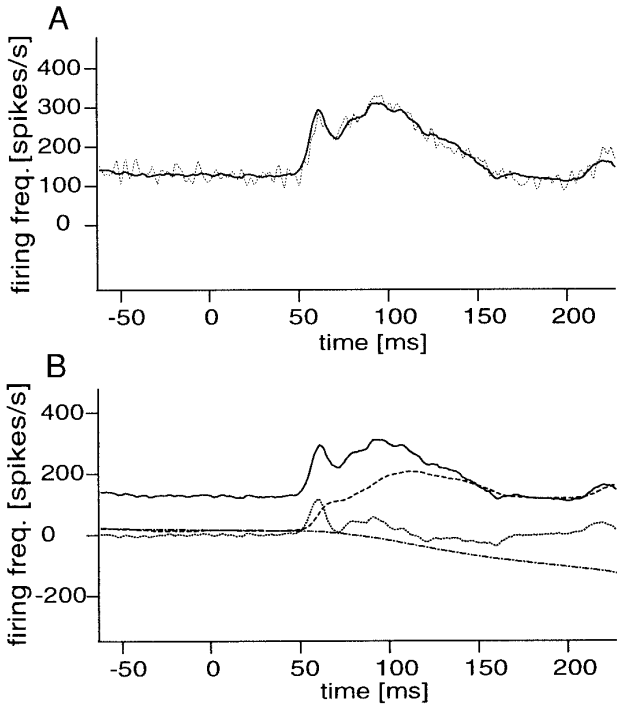

FIG. 3. *A*: reconstructed (solid line) and observed (dotted line) ventral paraflocculus (VPFL) P-cell firing patterns (preferred direction stimulus, 40°/s). *B*: components of the reconstructed firing frequency ascribed to eye angular acceleration (dotted line), angular velocity (dashed line), and angular position (dashdot line). Estimated coefficients are given in the text.

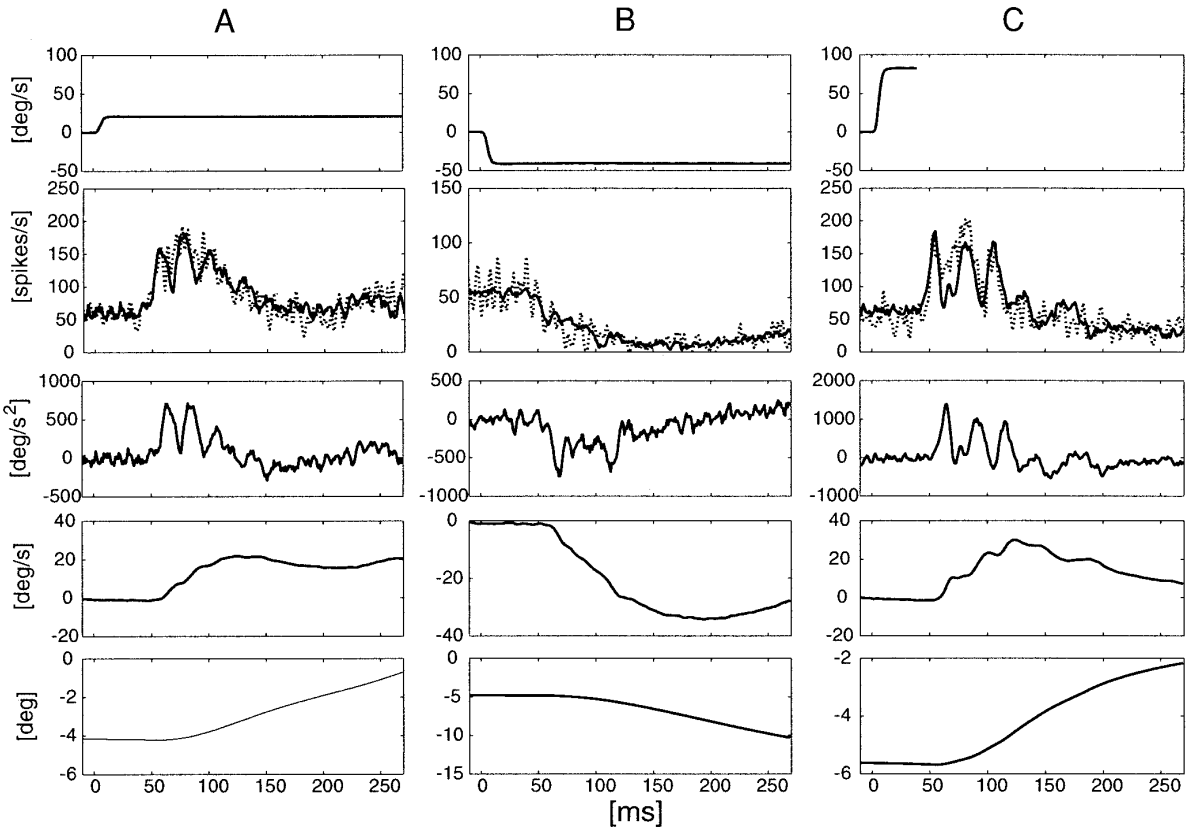

FIG. 4. From *top* to *bottom*: stimulus velocity, observed and reconstructed firing frequency, eye angular acceleration, angular velocity, and angular position under a preferred direction stimulus condition (*A;* 20°/s): CD = 0.73, M = 0.122, B = 2.70, K = −16.6, δ = 8 ms; an antipreferred direction stimulus condition (*B;* −40°/s): CD = 0.79, M = 0.0303, B = 1.36, K = 1.04, δ = 10 ms; and duration change stimulus condition (*C;* 40 ms): CD = 0.72, M = 0.0782, B = 1.51, K = −12.0, δ = 10 ms.

tation satisfactorily predicted the complex time course of the P-cell firing. Figure 3*B* shows the temporal patterns of the components decomposed into the acceleration, velocity, position, and bias terms of *Eq. 1.* Although the acceleration coefficient (M) was small, its component $M\ddot{\theta}(t)$ was predominant in the initial phase of the response as shown in this figure, and its velocity component $B\dot{\theta}(t)$ was dominant in most of the rest. After the initial phase, the acceleration component decreased and the position component $K\theta(t)$ increased. The position component, however, had reversed sign relative to the direction of the movements.

Figure 4 shows other examples from another cell. Figure 4*A* shows, for a preferred direction stimulus (20 deg/s), the reconstructed firing pattern (solid line), which was close to the observed firing pattern (dotted line). The CD was not very high (CD = 0.73) because of a lot of sampling noise. For an antipreferred direction stimulus (−40 deg/s; Fig. 4*B*), the firing frequency decreased relative to the spontaneous level. Because of the high spontaneous level (~50 spikes/s in this case), the firing pattern was reconstructed well from the eye movement (CD = 0.79). For a short stimulus (occluded by a mechanical shutter 40 ms after the stimulus onset; Fig. 4*C*), the P cell firing quickly decayed. This firing pattern was different from the previous two cases, but also was reconstructed well from the eye movement (CD = 0.72).

MODELING CHECK AND DATA CLASSIFICATION. By statistically analyzing the reconstruction results for many VPFL P cells under several conditions, we examined the role of VPFL P cells in the ocular following response. As noted in METHODS, three major reasons could lead to unsuccessful parameter estimation: inapplicable model, a low S:N ratio of the firing frequency (because of small number of averaging trials or insufficient modulation by an ineffective stimulus), and high correlations among the acceleration, velocity, and position signals. To characterize neural activities, reliable parameter estimation would be required. Employing the procedure described in METHODS, we classified all of the data sets into *data groups* [*i*]–[*v*] shown in Fig. 2.

When residual errors were checked with the autocorrelation method (APPENDIX A), the inverse dynamics representation (*Eq. 1*) was found to be inapplicable only for small number of P cell firing patterns (24/232), indicating the generality of this model. Figure 5 shows the frequency histogram of the coefficients of determination (CD) for the 208 (232−24) data sets belonging to *groups* [*i*], [*ii*], [*iv*], and [*v*] in Fig. 2.

In light of the second reason for unsuccessful estimations noted earlier, we need to avoid unreliable parameters estimated from data sets with low CD. By applying a threshold level of CD (0.6), 146 of 208 data sets (70.2%) were classified into the high S:N *data groups* [*iv*] and [*v*]. In regard

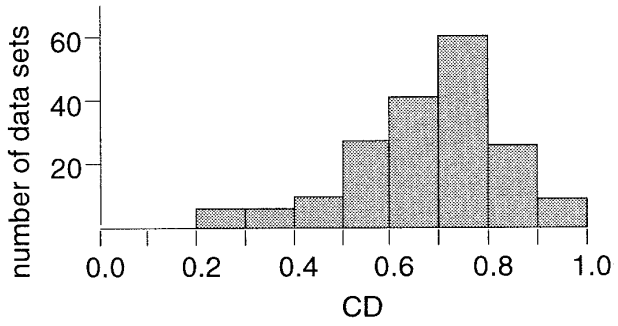

FIG. 5. Frequency histogram of the coefficient of determination (CD) for 208 data sets classified by the autocorrelation check.

to the third reason, the estimation reliabilities can be examined by a statistical index, confidence intervals (Hines and Montgomery 1972), for the linearly estimated parameters as checked later. For a time-lag parameter, however, we cannot obtain this index because of the nonlinear global search method. Thus by using the convexity of goodness-of-fit (procedure is described in APPENDIX C), we extracted 109 data sets, for which time lags were reliably estimated, from the 146 data sets.

Table 2 summarizes the classification for each stimulus condition. Note that, in each stimulus condition, the number of data sets is identical to the number of P cells. By combining the autocorrelation and the CD classifications, 62 data sets were classified as poorly modulated data (low S:N data, [*i*] and [*ii*]). As a result, the total number of well-modulated data (high S:N data [*iii*]–[*v*]) was 170. Thus 86% (146/170) of the data with high S:N were reconstructed well, and reliable parameters were estimated for 64% (109/170) of the data with high S:N. As shown in Table 2, the percentage of the data sets classified in [*v*] are different under each stimulus condition. Especially, for the slow stimuli (−20, −10, 10°/s), the P cells were too weakly modulated, resulting in many data sets being classified into [*i*] and [*ii*]. On the contrary, for 160°/s stimulus, one-half of the data sets (11/21) were classified into [*iii*], suggesting a nonlinear relationship between P cell firing and OFR as discussed later.

ESTIMATED LATENCY AND COEFFICIENTS. From the estimated parameters of the 109 data sets from 28 P cells among all 30 cells classified into [*v*], we here characterize the local relationship between P cell firing and eye movement. The histogram and the quantile box plot of estimated time lags for these 109 data sets are shown in Fig. 6*A*. The mean time lag was 7.47 ± 4.23 (SD) ms. For 54.1% of the data sets (59/109) taken from 22 cells, the estimated time lag was between 8 and 11 ms, which was very close to the latency of movements elicited by an electrical stimulus derived to VPFL (8.6–10.9 ms) (Shidara and Kawano 1993). This satisfies the prerequisite for firing frequency to represent the motor command. Extreme positive or negative time lags were potentially caused, respectively, by longer transmission times or because the discharges were generated by oculomotor feedback signals.

The histograms and quantile box plots of estimated coefficients of acceleration, velocity and position for the 109 data sets belonging to [*v*] are shown in Fig. 6, *B*–*D*, and their means and standard deviations are summarized in Table 3*A*. The mean confidence intervals (95%) for the coefficients (*M*, *B*, and *K*) were 0.0225 ± 0.00833 (spikes/s)/(deg/s^2), 0.610 ± 0.230 (spikes/s)/(deg/s), and 5.23 ± 1.93 (spikes/s)/deg, respectively. These confidence intervals were several times smaller than the variances of each estimated coefficient listed in Table 3*A*, indicating sufficient estimation reliability. The histograms of all coefficients had single peaks and had few extreme values, indicating that the relationships between P cell firing and eye movements were roughly similar under any condition, and that the averaged coefficients might represent the global average behavior of VPFL activity during OFR with a wide variety of stimulus dimensions.

As shown in Table 3*B*, however, these coefficients have different trends in the three applied conditions (preferred and antipreferred directions and duration). The magnitudes of the coefficients of acceleration, velocity, and position for the stimuli in the preferred direction were frequently larger than those in the antipreferred direction. This tendency can be clearly observed in the individual P cells as shown in Fig. 7*A*, in which the coefficients of seven P cells under the stimulus speeds of 40 and −40°/s were compared. This observation is consistent with the finding in a different kind of eye movement (vestibuloocular reflex) that the change in P cell firing for a stimulus in the preferred direction is greater than that in the antipreferred direction (Lisberger et al. 1994). To show the change in coefficients at each stimulus speed, the coefficient values of the data sets in [*v*] are plotted against stimulus speed in Fig. 7*B*. Each line merges the estimated coefficients for an individual P cell under sev-

TABLE 2. *Number of classified cells and total data sets in the local analysis*

Stimulus Condition	All	[*i*] + [*ii*]	[*iii*]	[*iv*]	[*v*]
Speed, deg/s					
−160	15	5	1	2	7
−80	19	4	1	4	10
−40	15	3	0	0	12
−20	15	6	1	3	5
−10	15	9	0	4	2
10	22	10	0	4	8
20	22	6	0	3	13
40	22	2	1	2	17
80	28	2	5	6	15
160	21	1	11	3	6
Duration, ms					
10	7	5	0	0	2
20	7	3	0	0	4
40	6	3	1	0	2
60	6	2	1	1	2
80	6	1	1	2	2
160	6	0	1	3	2
Total (data sets)	232	62	24	37	109
Subtotal for [*iv*] + [*v*]				146	
Subtotal for [*iii*] + [*iv*] + [*v*]				170	

In the first column, each number denotes the stimulus speed or stimulus duration. The number of the cells prepared under each stimulus condition is in the second left column. All numbers shown in the remaining columns indicate the number of data sets classified with the statistical methods (see text).

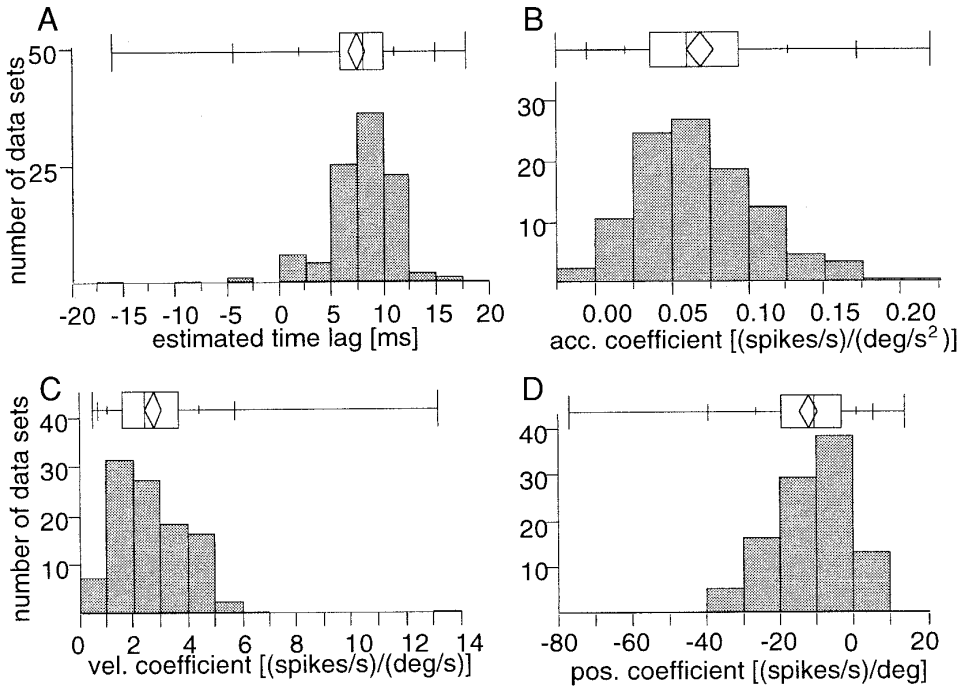

FIG. 6. Frequency histogram and quantile box plot of estimated time-lags (*A*), acceleration coefficients (*B*), velocity coefficients (*C*), and positional coefficients (*D*) of 109 data sets for which the estimated parameters are reliable (i.e., the data sets in *group* [*v*]). Quantile box shows the median as a line across the middle and the quartiles (25th and 75th percentiles) as its ends. Diamond identifies the mean of the samples and the 95% confidence interval about the mean.

eral speeds. For acceleration (*M* in Fig. 7*B*), the coefficients in the negative (antipreferred) direction were smaller than those in the positive (preferred) direction, and there were no general trends in the positive direction. The magnitude of the coefficients of velocity and position (*B* and *K* in Fig. 7*B*) tended to reduce as the stimulus velocity increased in the positive direction. For example, the coefficients for a 20°/s stimulus were significantly larger (*t*-test 95%) than those for an 80°/s stimulus in the most of the P cells successfully reconstructed (9/11 cells for velocity coefficient, 10/11 cells for position coefficient). In the negative direction, this trend was weaker, although found in several P cells. In summary, firing frequencies in the local conditions were reconstructed successfully using a linear model, and some coefficients differed for different stimulus conditions.

Global condition analysis

RECONSTRUCTION OF P CELL FIRING FREQUENCY. In the above local condition analyses, coefficient changes for different stimuli suggested nonlinear relationships between P cell firing and OFR. However, the significance of the nonlinearity in the global conditions cannot be evaluated only by the coefficient difference in the local condition analyses because of the different sensitivities of parameters. To examine the generality of the model (*Eq. 1*) and to characterize the global relationship between P cell and OFR, global fitting for multiple stimulus conditions was applied. Figure 8*A* shows for one of the fitting examples (*top* to *bottom*) stimulus velocity patterns, observed single P cell firing frequency patterns (gray line) superimposed on the reconstructed one

TABLE 3. *Mean and standard deviation of estimated coefficients and time lags in the local analysis*

A. Variances

Coefficients	Time Lag
M, (spikes/s)/(deg/s²)	0.0694 ± 0.0434
B, (spikes/s)/(deg/s)	2.76 ± 1.63
K, (spikes/s)/deg	−12.2 ± 12.8
δ, ms	7.50 ± 4.24

B. Stimulus Conditions

	Preferred Direction	Antipreferred Direction	Duration
M, (spikes/s)/(deg/s²)	0.0882 ± 0.0446	0.0409 ± 0.0270	0.0633 ± 0.0304
B, (spikes/s)/(deg/s)	3.39 ± 1.79	1.94 ± 0.91	2.24 ± 1.31
K, (spikes/s)/deg	−18.0 ± 13.5	−2.32 ± 5.32	−13.3 ± 6.32
δ, ms	8.51 ± 1.99	5.53 ± 6.45	8.29 ± 1.90

Values are means ± SD. Data are from 109 data sets (from 28 cells). Those in A are classified into data group [*v*].

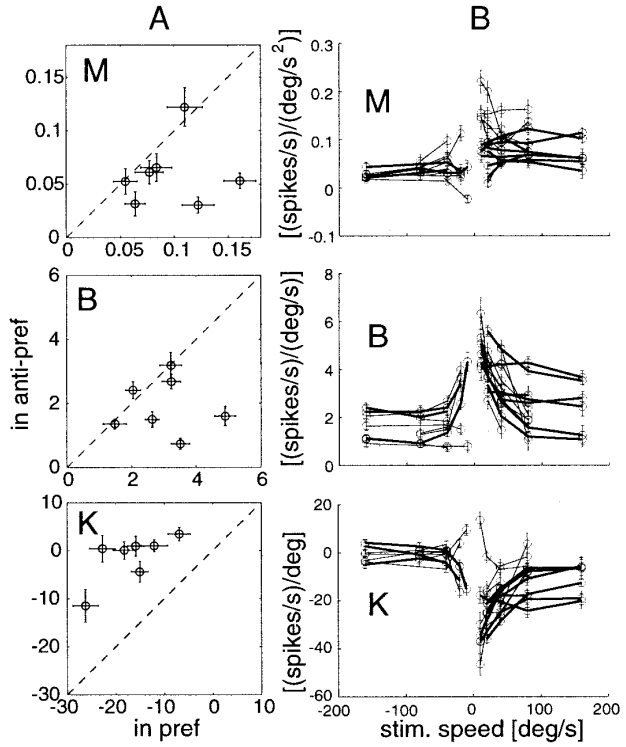

FIG. 7. *A*: comparison between estimated coefficients under preferred and antipreferred direction stimulus conditions (−40 and 40°/s) for 7 P cells. Each dotted line denotes equal coefficient in preferred and antipreferred direction stimuli, and each open circle is estimated values and cross denotes confidence intervals (95%) of estimates for preferred and antipreferred direction stimuli; *M*, acceleration coefficient; *B*, velocity coefficient; *K*, position coefficient. *B*: estimated coefficients under the various stimulus speed conditions. Each line merges the estimated coefficients for each P cell under several speed stimuli. Thick lines denote the P cells for which global fittings were successful for the preferred or antipreferred direction stimuli.

(solid line), eye acceleration, eye velocity, and eye position patterns under five different stimulus velocities in the preferred direction. The P cell firing frequency patterns were reconstructed by one parameter set of *Eq. 1* for all five stimulus conditions, and were in good agreement with the observed firing patterns. The CD was 0.84, indicating that the simple linear inverse-dynamics representation could satisfactorily predict complex time courses of P cell firing in the global as well as the local fitting. Figure 8*B* (different cell from Fig. 8*A*) shows stimulus velocities in the antipreferred direction (*top*) and observed firing frequencies (gray line) and reconstructed firing frequencies (solid line; *bottom*; CD = 0.75). Figure 8*C* shows records for a different cell in a duration change condition in the same manner (CD = 0.78; see the figure caption for the estimated parameters). These successful reconstructions by one parameter set indicate that the activities of these P cells were almost linearly correlated with simultaneously observed eye movements under the limited multiple stimulus conditions employed.

MODELING CHECK AND ESTIMATED COEFFICIENTS. Next, we summarize the analyses of firing frequency patterns of each single P cell taken under multiple conditions using one parameter set. The firing patterns observed in a single P cell were categorized into several groups by stimulus conditions: the preferred direction stimuli, the antipreferred direction stimuli, the change in stimulus duration, the preferred direction stimuli and antipreferred direction stimuli, and the preferred direction stimuli and change in stimulus duration. The same statistical methods used in the local data analysis were applied to classify the data. Table 4 shows the number of the data sets (identical to the number of cells) classified into each group in the same manner as in Table 2. For 13 of 21 data sets (13 cells) with high S:N ratio under the first stimulus condition (the preferred direction stimuli), the firing patterns were reconstructed well using a single set of parameters in the linear inverse representation. Similarly, 3/7, 5/6, 5/15, and 2/5 cells with high S:N ratio ([*iii*], [*iv*], and [*v*]) were reconstructed well using a single set of parameters for the second through fifth, respectively, global stimulus conditions. The few successful reconstructions made under the second, fourth, and fifth global conditions indicate that some global nonlinearities degrade the linear regression estimation. This will be further discussed later.

The average estimated coefficients and time lags of the data sets belonging to [*v*] under the three conditions (preferred direction, antipreferred direction, duration) (Table 5) were close to those estimated in the local analysis (Table 3*A*). This suggests that the averaged estimated coefficients in the local analysis roughly represent the global behavior of VPFL during OFR.

DOES THE P CELL ENCODE THE JERK OF OFR? In many of the previous studies on modeling and analyzing relationships between slow eye movements and the activity of eye motor neurons or related brain regions, first-order linear systems with position and velocity terms were used. This was probably because the inertia of the eyeball is negligibly small and because the frequency responses between the activity of eye motor neurons and the eye movements could be fitted well by a first-order system with delay (Reinhart and Zuber 1970). On the other hand, Robinson (1965) proposed a higher-order model from the viewpoint of the mechanical properties of the eye system. Several studies (Fuchs et al. 1988; Keller 1973) also indicate that a second-order model is necessary for explaining the firing frequencies in motoneurons. Even in the cerebellum, acceleration properties were encoded by the P cells in the initial phase of slow eye movements (Stone and Lisberger 1990). In addition, as shown above, we have successfully reconstructed P cell firing waveforms by using a second-order linear inverse dynamics representation (*Eq. 1*).

How can we determine the differential order suitable for analyzing the relations between neural activities and eye movements? To statistically examine the model applicability for identifying relationships between P-cell outputs and eye movements, we will apply two methods, the *t*-test and Cp statistics, to the following third-order model having jerk, acceleration, velocity, position, and bias terms with time lag

$$\hat{f}(t-\delta) = J\dddot{\theta}(t) + M\ddot{\theta}(t) + B\dot{\theta}(t) + K\theta(t) + f_{\text{bias}} \qquad (3)$$

Here $\hat{f}$ denotes the reconstructed firing frequency of the P cell at $t - \delta$; f_{bias} denotes the bias; and *J*, *M*, *B*, and *K*, respectively, denote the jerk, acceleration, velocity, and positional coefficients.

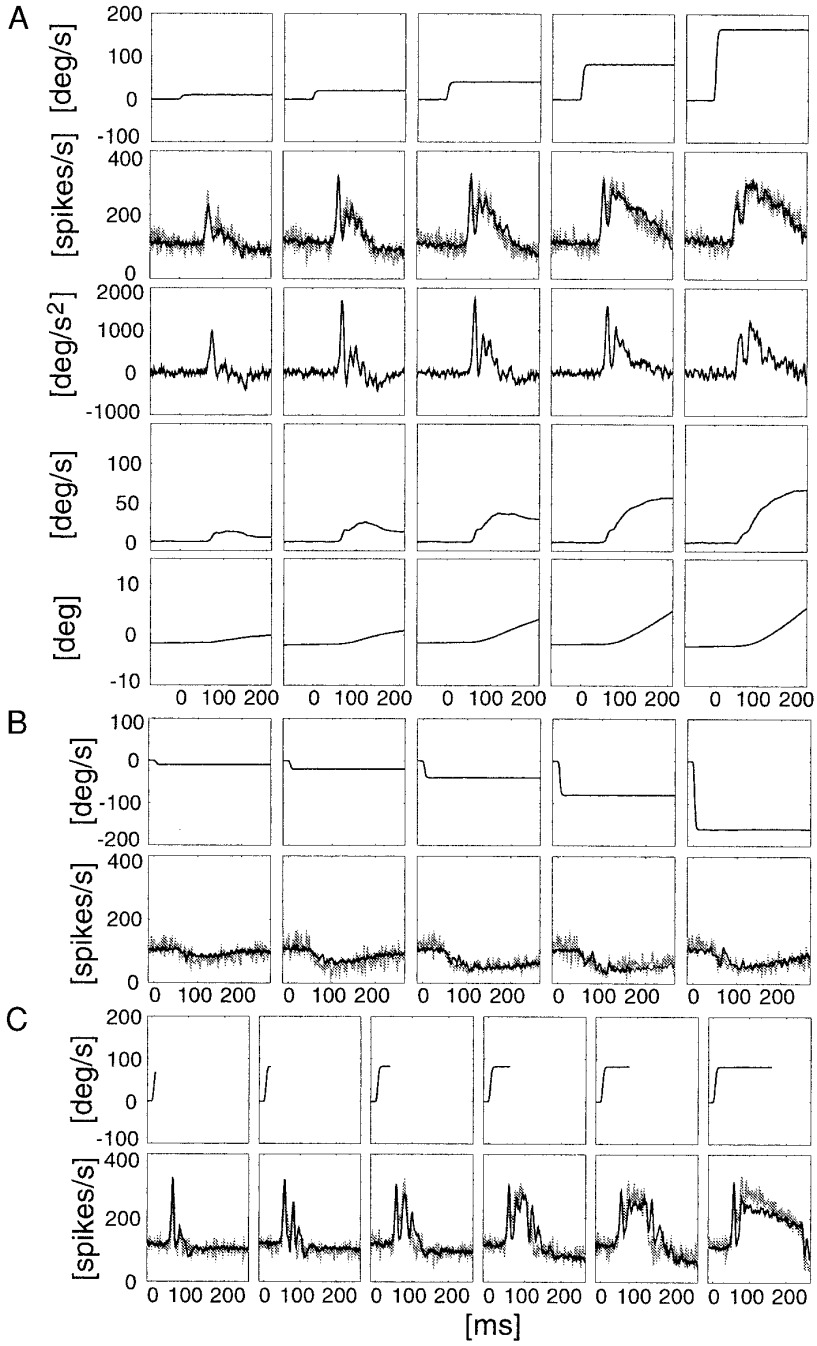

FIG. 8. *A*: from the *top* to *bottom*: stimulus velocity patterns, observed single P cell firing frequency patterns (gray line), eye acceleration patterns, eye velocity patterns, and eye position patterns under 5 different stimulus velocities in the preferred direction. Reconstructed P cell firing frequency patterns of 1 parameter set (i.e., global fitting) have been superimposed in the graphs in the 2nd row (solid line). *B*: antipreferred direction stimulus conditions. *C*: duration change stimulus conditions. *Top graphs* in *B* and *C* show the stimulus velocities. *Bottom graphs*: observed firing frequencies (gray line) and reconstructed firing frequencies (solid line) of 1 parameter set. Estimated coefficients and time lags were *A*: $M = 0.108$ (spikes/s)/(deg/s^2), $B = 2.92$ (spikes/s)/(deg/s), $K = -23.0$ (spikes/s)/deg, and $\delta = 8$ ms; *B*: $M = 0.0640$, $B = 1.72$, $K = 1.35$, and $\delta = 6$; *C*: $M = 0.100$, $B = 2.31$, $K = -9.58$, and $\delta = 9$.

First, the original 232 data sets were again analyzed with *Eq. 3* instead of *Eq. 1*. Then 113 data sets were classified into the *data group* [*v*] by the combination check. The necessity of each component on the right side of *Eq. 3* was examined by the *t*-test for the null hypothesis that the coefficient of each component is zero. The numbers of data sets classified by the *P* value of the *t*-test are listed in Table 6. In many of the cases (89/113), the null hypothesis for the jerk component was not rejected ($0.05 \leq P$). This result indicates that the jerk component is unnecessary for the majority of firing patterns. On the other hand, the small *P* value for the other components (i.e., acceleration, velocity, positional, and bias components) indicates that these components are necessary for adequate reconstruction.

TABLE 4. *Classified cells in the global analysis*

Stimulus Condition	All	[*i*] + [*ii*]	[*iii*]	[*iv*]	[*v*]
Preferred direction	21	0	8	4	9
Antipreferred direction	15	8	4	0	3
Duration	6	0	1	3	2
Preferred + antipreferred	15	0	10	4	1
Preferred + duration	5	0	3	1	1

Values are numbers of cells.

TABLE 5. *Mean estimated coefficients and time-lag values for three conditions in global fitting*

	Averaged Estimated Coefficients and Time Lag*		
	Preferred	Antipreferred	Duration
M, (spikes/s)/(deg/s^2)	0.0666	0.0320	0.0740
B, (spikes/s)/(deg/s)	2.63	2.21	2.79
K, (spikes/s)/deg	−15.1	−4.12	−6.09
δ, ms	7.33	6.00	9.00

* Preferred, preferred direction stimulus condition; antipreferred, antipreferred stimulus direction condition; duration, stimulus duration change condition.

Furthermore, we examined the Cp statistics values of the 113 data sets using four potential models: *1*) a velocity, position, and bias model; *2*) an acceleration, velocity, and bias model; *3*) an acceleration, velocity, position, and bias model; and *4*) a jerk, acceleration, velocity, position, and bias model. According to Hines and Montgomery (1972), the estimated variance of the full term model (*4*) was used as the estimated population variance. The Cp statistics value was minimum for *model 3* in 77.9% of the data sets (88/113) (*1*: 0%; *2*: 7.1%; *4*: 15%). This result is consistent with that of the *t*-test and indicates that the jerk term in *Eq. 3* is unnecessary for the majority of firing patterns, whereas the other terms are required to describe the relationship between the P cell firing and eye movement. Note that, although *model 4* was selected in 15% data, the Cp-statistics values of those data for *model 3* (9.3 ± 4.3) were close to those for *model 4* (5.0), whereas those for *models 1* and *2* were 159.0 and 82.4, respectively, in mean. This indicates that the advantage of *model 4* is small even for these 15% data.

NONLINEARITY BETWEEN P CELL FIRING AND OFR. The local analysis suggested that the linear relationship between P cell activity and eye movement is sometimes violated under high-speed (160°/s) stimulus conditions. We here examine how the visual-stimulus speed, P cell firing frequency, and eye movement relate to each other. Figure 9*A* shows the relationships between the stimulus speed and root mean squared firing frequency (spontaneous firing level was subtracted) of 21 P cells in the preferred stimulus direction (positive speed) and of 15 P cells in the antipreferred stimulus direction (negative speed). As observed by Shidara, Kawano, Gomi, and Kawato (1993) and as shown in Fig. 9*A*, the firing frequencies saturated at higher stimulus speeds, indicating that some nonlinear factors are present between the stimulus speeds and firing frequencies.

By contrast, the relationships between the spike firing

TABLE 6. *Significance of each component in the reconstructed firing frequency*

	Number of Data Sets		
	$P < 0.005$	$0.005 < P < 0.05$	$0.05 < P$
Jerk component	12	12	89
Acceleration component	101	3	9
Velocity component	112	1	0
Positional component	95	3	15

The P values of the *t*-test indicate the significance probability of the null hypothesis that the coefficient of each component is zero. If the P value is very small, model fitting is performed poorly when that component is dropped.

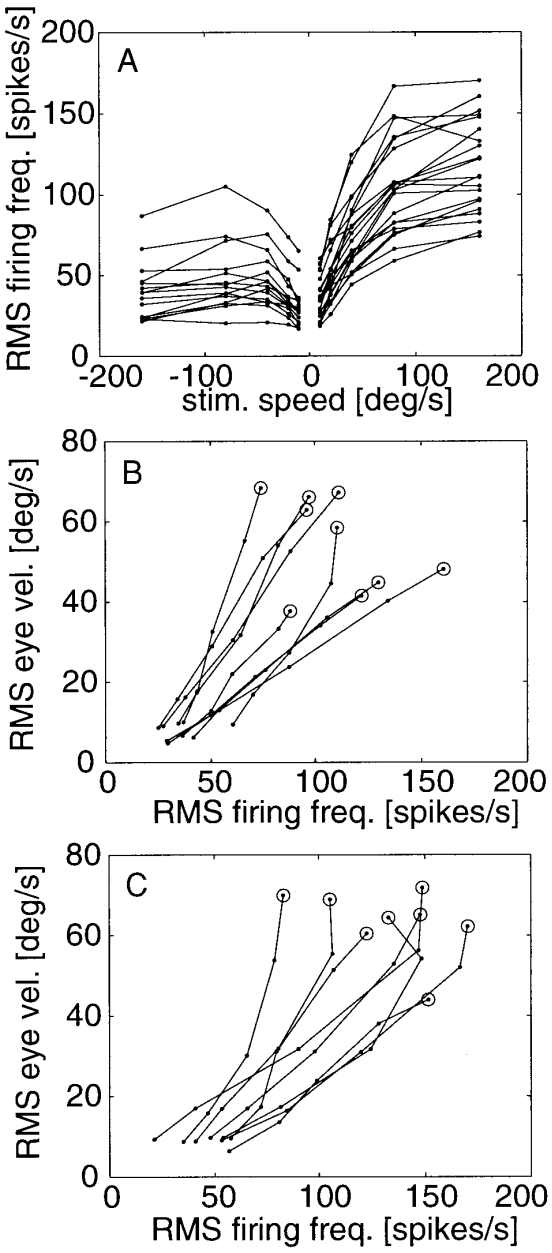

FIG. 9. *A*: relationships between stimulus speed and the root mean squared (RMS) firing frequency (spontaneous firing level was subtracted) of 21 P cells for the preferred stimulus direction (positive speed) and of 15 P cells for the antipreferred stimulus direction (negative speed). Each line merges the data for a single P cell in different stimulus speeds. *B*: relationships between the RMS firing frequency and the RMS eye velocity under the preferred direction stimulus conditions (see Table 5), for 9 P cells that were classified into *data group* [*v*] in global fitting. *C*: those relations for the 8 P cells classified into *data group* [*iii*]. In *B* and *C*, dots indicate the data points under different speed conditions; ○, data points for a stimulus speed of 160°/s.

frequencies and the eye movements were much more linear. Figure 9, *B* and *C*, depict the relationship between the root mean squared firing frequency and eye velocity of 21 P cells under preferred direction stimulus conditions (see Table 4). The dots indicate data points under different stimulus speed conditions (10–160°/s; ○, 160°/s). In Fig. 9*B*, eye velocities increase linearly with firing frequency for eight of those nine P cells in which global fitting was successful (see Table 4 [*v*] for preferred stimulus direction). On the other hand, as shown in Fig. 9*C*, the linearities of the other P cells (8 cells for which global fitting did not succeed. See Table 4 [*iii*] for preferred stimulus direction) were violated, especially concerning the 160°/s stimuli. Note that, in all eight cells, the P cell firing patterns for the 160°/s preferred direction stimulus also could not be modeled by the local fitting (i.e., classified into [*iii*] of Table 2), whereas nonlinearity was not found (i.e., not classified into [*iii*]) for most other stimulus conditions (36/40 in 8 cells). These nonlinearities may have been caused by activity saturation and may be one of the main reasons for poor fitting in the global conditions in the preferred direction (see Table 4 [*iii*]). Even though some P cells were saturated for the fast stimuli, because of the spatial summations of many P cells (i.e., population coding) for driving the eye movement, the eye velocity was increased by increased activity in those P cells not saturated for the fast stimuli as sampled in Fig. 9*B*.

In addition to this nonlinearity under the high-speed stimulus observed in some cells, parameter changes for different stimuli, as observed in Fig. 7, also indicated nonlinearity. However, as mentioned above, parameter changes in the local fitting do not directly imply unsuccessful reconstruction in the global condition. In fact, as shown in Fig. 7, the best-fit parameters did change under different stimulus speeds even for the nine cells with successful reconstruction in the global fitting, the local parameters of which were merged by thick lines. Thus the saturation for high-speed stimuli rather than the parameter changes for slow speed stimuli was a dominant factor leading to unsuccessful reconstruction in the global fitting in preferred direction of the eight cells.

DISCUSSION

Contributions of VPFL P cell to OFR

The acceleration and velocity coefficients shown in the present paper indicate that the P cell firing encodes the dynamic component of the motor command for OFR. Similar observations in VPFL have been reported for smooth pursuit (Miles et al. 1980; Stone and Lisberger 1990). The firing frequency sensitivity of the ''gaze-velocity P cell'' in VPFL with respect to the eye velocity has been summarized as 1.02 (0.21–2.86) (spikes/s)/(deg/s) (ipsi) in Miles et al. (1980) and as 1.34 (0.46–2.94) (spikes/s)/(deg/s) (down) and 0.99 (0.21–3.16) (spikes/s)/(deg/s) (ipsi) in Stone and Lisberger (1990). These values have a similar range but are slightly smaller than the eye-velocity sensitivities (i.e., the velocity coefficients) in our analysis.

As for the positional component, it has been reported that the VPFL P cell activities during eye fixation were correlated positively with eye position although these correlations were very weak [ipsi: 0.26 (spikes/s)/deg, max. 0.87; contra: 0.17 (spikes/s)/deg, max. 0.62] (Miles et al. 1980). In addition, it has been reported (Krauzlis and Lisberger 1994) that, in a simulation study, the horizontal smooth pursuit eye movement could be reconstructed from the averaged activities of the ipsilateral and contralateral VPFL P cells with pulse (proportion), step (integration), and slide (low-pass filtering) processing, indicating weak or no correlation with eye position.

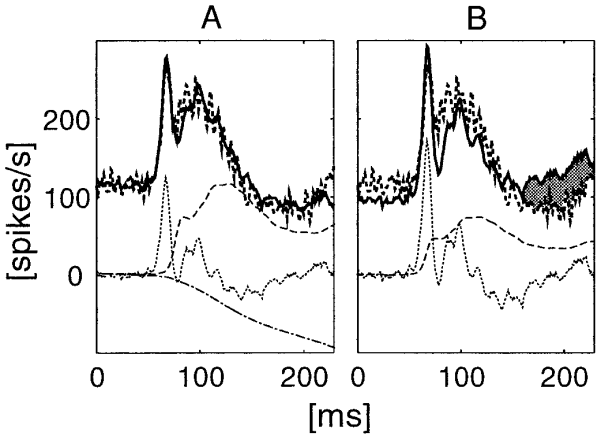

FIG. 10. Observed P cell firing frequencies (thick dashed line) and reconstructed firing frequencies (thick solid lines) of a regression model with acceleration velocity, position, and bias terms (*A; M* = 0.0807, *B* = 4.69, and *K* = −31.4) and a regression model with acceleration, velocity, and bias terms (*B; M* = 0.111 and *B* = 3.00). The remarkable residual error indicated by the shadow was observed when using the model without a positional term. Thin dotted line denotes acceleration component, thin dashed line denotes velocity component, and thin dashdot line denotes positional component.

By contrast, as shown in Fig. 3*B* and the preceding analysis, many VPFL P cell activities during OFR are correlated negatively with eye position to an extent that is not negligible. For example, the fitting performance obtained using a model without a positional component was degraded as shown in Fig. 10*B*, whereas the firing pattern was well reconstructed by the model including the positional component expressed by *Eq. 1* (see Fig. 10*A*). Comparing Fig. 10, *B* with *A*, especially in the latter phase, the firing pattern in *B* was poorly reconstructed, indicating the importance of the positional component for this P cell. Although negative correlation with position was found for many P cell firings as shown in Fig. 6*D*, positive correlation and no correlation also were observed in several cases. This finding is consistent with experimental results (Zhang et al. 1995) in which some of the flocculus target neurons in the vestibular nucleus had the preferred direction in position opposite to that in velocity, while the firings of other neurons were not correlated with position.

On the other hand, it has been reported (Keller 1973) that the firing frequency for eye motor neurons is correlated positively with eye position in any type of eye movement. Considering this fact, the eye movement cannot be executed only as a result of the P cell firing that we observed because of its lack of an adequate positional component. Other input

to the downstream neural circuit presumably contribute to driving the eye movements.

Cerebellum as a dynamic motor command generator

Several studies (Kawano et al. 1992, 1994; Shidara et al. 1993) suggest that the neural firings in the MST and DLPN, which are located upstream of the VPFL, encode visual input signals during OFR and that the VPFL P cells send eye-driving signals. Although the fact that VPFL P cells send the signals to eye motor neurons was confirmed in an electrical stimulation experiment (Shidara and Kawano 1993), the sensitivity coefficients in the two activities cannot be directly compared because the firing frequency levels are different in P cells and in motor neurons. Rather we should compare the ratios of mean coefficients in both regions.

The ratio of the mean acceleration coefficient to the mean velocity coefficient ($E[B]:E[B]$) for the 109 data sets from 28 cells listed in Table 3*A* is 0.0251. This ratio is close to, but slightly larger than, that of extraocular motor neurons (0.015), calculated from the averaged time constants of the 15 cases observed in Keller (1973). Because the acceleration and velocity coefficients were distributed normally around each mean value rather than uniformly distributed, this similarity in the coefficient ratio might suggest that the P cells observed here were sufficient to provide the dynamic component of the eye movement, although the positional component should be produced elsewhere such as in other brain regions, a downstream neural structure, or other types of P cells. A potential configuration of the cerebellar internal model is that the full dynamics computation is constituted by several complementary internal models (e.g., inverse dynamics model and inverse statics model) working together in parallel as demonstrated in Katayama and Kawato (1991).

Note that these discussions are based on the decoding of ensemble activity in each P cell. This is reasonable because the spatial averaging of many P cell outputs either at the brain stem level or at the motor neurons can replace the ensemble averaging of firing patterns. Suppose that the synaptic weights from many VPFL P cells to the brain stem neuron distribute randomly. Then the firing pattern of this brain stem neuron roughly encodes the spatial averaging of the temporal firing frequencies the P cells innervating it.

As for the upstream side, the preferred directions in the DLPN and MST are spread in all directions (Kawano et al. 1992, 1994), whereas those in the VPFL are only ipsiversive and downward (Shidara and Kawano 1993). The firing temporal patterns are also different in each region: the acceleration component of the firing was more evident in the DLPN and MST than in the VPFL as quantitatively demonstrated in our recent study (Takemura et al. 1994). These facts imply that the cerebellum is the main site of sensory-motor transformation. However, the details of the functional transformation in the cerebellum are still unclear. To examine the computational functions of the cerebellum, we need to clarify what information is encoded in the inputs to the cerebellum.

Stone and Lisberger (1990) pointed out the importance of eye-velocity positive feedback to P cells (carried by corollary discharge) rather than visual input (retinal error) sometime after the initiation of pursuit. They showed persistent firing of P cells during smooth pursuit with no retinal error while the targets were stabilized on the fovea by servo control, and they concluded that these sustained responses are driven by eye-velocity inputs. The observations of Newsome et al. (1988) and Kawano et al. (1994), however, are consistent with another possibility. When the visual target vanished for a brief period during smooth pursuit eye movement, the eye tracked the invisible target trajectory for a while (Stone and Lisberger 1990) or slowed down slightly (Becker and Fuchs 1985; Kawano et al. 1994). During this time, not only VPFL P cells (Stone and Lisberger 1990) but also MST neurons (Newsome et al. 1988; Sakata et al. 1983) continued firing or slowly decreased their firing (Kawano et al. 1994) with no retinal slip signal. Thus the MST output does not encode simple retinal slip signals; rather, it might encode a kind of desired or predicted target movement. On the other hand, when the visual stimulus (random dot pattern) vanished during OFR, both the firing of the VPFL P cells (cf. Fig. 8*C*) and that of the DLPN neurons (Kawano et al. 1992), which received signals from MST decayed quickly, and the eye movement suddenly slowed down.

These observations suggest that the dominant input signals to the VPFL might be signals from the higher CNS upstream of VPFL rather than feedback signals (such as corollary discharge signals), even in the sustained phase of the movement. If the desired eye movements are sent from regions upstream of the cerebellum, the hypothesis that the cerebellum computes a dominant part of the inverse dynamics for motion control (Gomi and Kawato 1992; Kawato and Gomi 1992a,b; Kawato et al. 1987) would be supported as one of the computational principles in the cerebellum.

APPENDIX A. COEFFICIENT OF DETERMINATION (CD) CHECK

A performance index *coefficient of determination* (Hines and Montgomery 1972) (CD) expressed in *Eq. A1* was evaluated to examine the applicability of the model and to guarantee the reliability of the estimated parameters.

$$\mathrm{CD} = 1 - \{\sum_t [\hat{f}(t) - f(t)]^2 / \sum_t [f(t) - \bar{f}]^2\} \qquad (A1)$$

Here $\hat{f}(t)$ is the reconstructed P-cell firing frequency and $f(t)$ denotes the observed firing frequency pattern. $\bar{f}$ is the temporal averaged firing frequency, which is constant over time. The index, CD, takes the range $0 \leq \mathrm{CD} \leq 1$, and comes close to 1 when the reconstructed firing frequency is close to the observed one. If the firing frequency is not linearly correlated with eye acceleration, velocity, or position, this index comes close to 0. This index equals the *correlation coefficient* squared.

APPENDIX B. AUTOCORRELATION CHECK

The first method focused on the residual error of the regression, which itself should not be correlated when the model was appropriate for representing the firing frequency. To avoid the filtering effect for residuals, we checked the autocorrelation function of the difference between the nonfiltered firing frequency, $f_{\mathrm{nf}}(t - t_f)$, and reconstructed firing frequency, $\hat{f}(t)$, as shown in the equation

$$C(\tau) = \frac{E_t[e(t) \cdot e(t + \tau)]}{\sqrt{E_t[e(t)^2] \cdot E_t[e(t + \tau)^2]}} \qquad (B1)$$

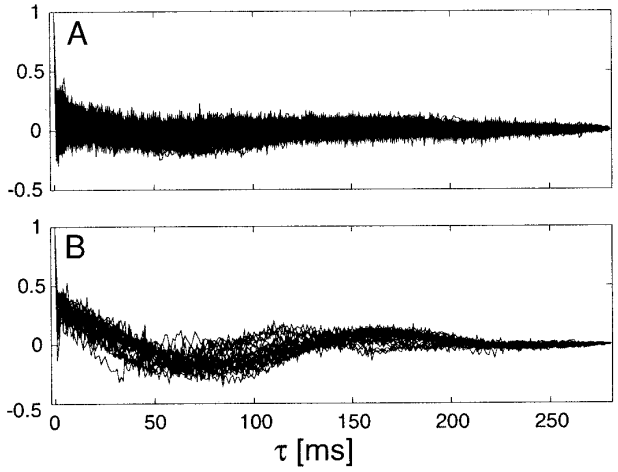

FIG. B1. Autocorrelation functions of the difference between nonfiltered firing frequencies $f_{nf}(t - t_f)$ and reconstructed firing frequencies $\hat{f}(t)$: for data sets for which the applied model was applicable (*A;* absolute threshold: 0.25 for the data over 10-ms difference), and for data sets for which the applied model was inapplicable (*B*).

Here, $E_t[\cdot]$ denotes the averaging in time t, and $e(t)$ denotes the difference between $f_{nf}(t - t_f)$ and $\hat{f}(t)$. t_f compensates the time delay caused by the filter for $\hat{f}(t)$ (in this case, $t_f = 2$ ms). If $e(t)$ can be regarded as random white noise, this autocorrelation function, $C(\tau)$, will be close to zero at all τ except $\tau = 0$. We can evaluate model applicability by checking these values. Figure B1*A* shows the autocorrelation functions of data sets classified into *data groups* [*i*], [*ii*], [*iv*], and [*v*] (208/232), and Fig. B1*B* shows those of the data sets classified into [*iii*] (24/232; threshold level was ±0.25 over 10 ms of τ). Most of the data sets were modeled successfully by *Eq. 1.*

APPENDIX C. TIME LAG CHECK

We applied a time lag test to guarantee the reliability of the estimated time lag δ. The function CD for time lags (from −20 to 20 ms) is termed CD_{TL}. The functional curve of the relationship between time lag and CD_{TL} should be convex near the maximum point in each data set if time lag is estimated reliably. To quantitatively evaluate this characteristic, the function between time lag and the CD_{TL} for each data set was shifted independently in both axes so that the maximum point of the CD_{TL} became the origin (i.e., 0 point). This procedure is expressed by *Eqs. C1* and *C2.* The function between the time lag and the CD_{TL} of *i*th P cell, Ψ, is expressed as

$$CD_{TL} = \Psi_i(TL) \qquad (C1)$$

Here, TL denotes the limited time range at 1-ms intervals from −20 to 20 ms, and CD_{TL} denotes the *coefficient of determination.* Let us replace CD_{TL} and TL with rCD_{TL} and rTL (relative CDTL and relative TL, respectively) as shown in the next equations to normalize the relationship between CD_{TL} and TL in each data set. CD_{max} denotes the maximum coefficient of determination in the limited range from −20 to 20 ms, and TL_{max} denotes the time lag at the CD_{max}

$$rCD_{TL} = CD_{TL} - CD_{max} \qquad (C2)$$

$$rTL = TL - TL_{max}$$

Figure C1*A* shows the relationships between time lag (TL) and coefficient of determination (CD_{TL}) for all of the data sets (146) chosen by the preceding tests (i.e., the autocorrelation test and the CD test). The normalized relationships between TL and CD_{TL} (rTL and rCD_{TL}) for these sets are superimposed in Fig. C1*B.* The horizontal axis represents the relative time lag (rTL), and the vertical axis represents the relative CD_{TL} (rCD_{TL}). To assort the

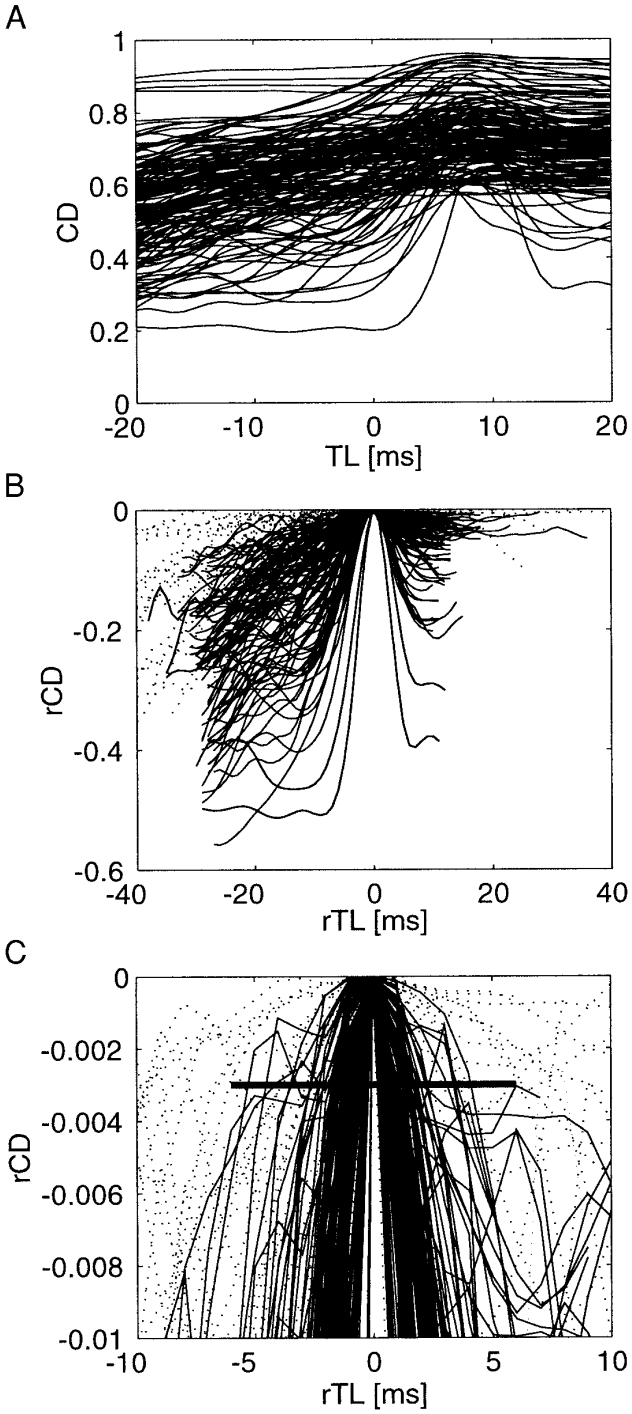

FIG. C1. *A*: relationships found between coefficient of determination (CD_{TL}) and time lag (TL) for 146 data sets, which were classified into [*iv*] or [*v*] by the autocorrelation check and CD check. Functions for all of the data sets (208) are superimposed. *B*: relationships between relative CD_{TL} (rCD_{TL}) and relative TL (rTL), for the same data sets. Solid lines denote relationships for the data sets classified into [*v*] by the time-lag check, and the dashed lines denote those for the data sets classified into [*iv*]. *C*: magnified view of the origin of *B* and the accept-window bar (±6 ms, −0.003).

data sets the CD_{TL} functions of which were sufficiently convex around the maximum, the accept window (± 6 ms, -0.003) indicated as a thick line in Fig. C1*C* was applied. As shown in Table 2, the 109 data sets were classified into *data group* [v].

We thank Drs. S. Yamane, Y. Tohkura, and M. Honda for continuing encouragement.

This work has been supported in part by grants to K. Kawano and M. Kawato from the Human Frontier Science Program.

Address for reprint requests: H. Gomi, NTT Basic Research Laboratories, Wakamiya 3-1, Morinosato, Atsugi, Kanagawa, 243-0198, Japan.

Received 29 December 1997; accepted in final form 3 April 1998.

REFERENCES

BECKER, W. AND FUCHS, A. F. Prediction in the oculomotor system: smooth pursuit during transient disappearance of a visual target. *Exp. Brain Res.* 57: 562–575, 1985.

BERTHIER, N. E., BARTO, A. G., AND MOORE, J. E. Linear systems analysis of the relationship between firing of deep cerebellar neurons and the classically conditioned nictitating membrane in rabbits. *Biol. Cybern.* 65: 99–105, 1991.

CHENEY, P. D. AND FETZ, E. E. Functional classes of primate corticomotoneuronal cells and their relation to active force. *J. Neurophysiol.* 44: 773–791, 1980.

CRAIG, J. J. *Introduction to Robotics: Mechanics and Control* (2nd ed.). Menlo Park, CA: Addison-Wesley Publishing, 1989.

EVARTS, E. V. Relation of pyramidal tract activity to force exerted during voluntary movement. *J. Neurophysiol.* 31: 14–27, 1968.

EVARTS, E. V. AND TANJI, J. Reflex and intended responses in motor cortex pyramidal tract neurons of monkey. *J. Neurophysiol.* 39: 1069–1080, 1976.

FUCHS, A. F., SCUDDER, C. A., AND KANEKO, R. S. Discharge patterns and recruitment order of identified motoneurons and internuclear neurons in the monkey abducens nucleus. *J. Neurophysiol.* 60: 1874–1895, 1988.

GEORGOPOULOS, A. P., KALASKA, J. F., CAMINITI, R., AND MASSEY, J. T. On the relations between the direction of two-dimensional arm movements and cell discharge in primate motor cortex. *J. Neurosci.* 2: 1527–1537, 1982.

GEORGOPOULOS, A. P., SCHWARTX, A. B., AND KETTNER, R. E. Neuronal population coding of movement direction. *Science* 233: 1416–1419, 1986.

GOMI, H. AND KAWATO, M. Adaptive feedback control models of the vestibulocerebellum and spinocerebellum. *Biol. Cybern.* 68: 105–114, 1992.

HINES, W. W. AND MONTGOMERY, D. C. *Probability and Statistics in Engineering and Management Science* (3rd ed.). New York: Wiley, 1972.

JUDGE, S. J., RICHMOND, B. J., AND CHU, F. C. Implantation of magnetic search coils for measurement of eye position: an improved method. *Vision Res.* 20: 535–538, 1980.

KALASKA, J. F., CAMINITI, R., AND GEORGOPOULOS, A. P. Cortical mechanisms related to the direction of two-dimensional arm movements: relations in parietal area 5 and comparison with motor cortex. *Exp. Brain Res.* 51: 247–260, 1983.

KATAYAMA, M. AND KAWATO, M. A parallel-hierarchical neural network model for motor control of musculo-skeletal system. *Syst. Comput. Jpn.* 22: 95–105, 1991.

KAWANO, K., SHIDARA, M., TAKEMURA, A., INOUE, Y., GOMI, H., AND KAWATO, M. Inverse-dynamics representation of eye movements by cerebellar purkinje cell activity during short-latency ocular-following responses. *Ann. NY Acad. Sci.* 781: 314–321, 1996.

KAWANO, K., SHIDARA, M., WATANABE, Y., AND YAMANE, S. Neural activity in cortical area MST of alert monkey during ocular following response. *J. Neurophysiol.* 71: 2305–2324, 1994.

KAWANO, K., SHIDARA, M., AND YAMANE, S. Neural activity in dorsolateral pontine nucleus of alert monkey during ocular following response. *J. Neurophysiol.* 67: 680–703, 1992.

KAWATO, M., FURUKAWA, K., AND SUZUKI, R. A hierarchical neural-network model for control and learning of voluntary movement. *Biol. Cybern.* 57: 169–185, 1987.

KAWATO, M. AND GOMI, H. The cerebellum and VOR/OKR learning models. *Trends Neurosci.* 15: 445–453, 1992a.

KAWATO, M. AND GOMI, H. A computational model of four regions of the cerebellum based on feedback-error learning. *Biol. Cybern.* 68: 95–103, 1992b.

KELLER, E. L. Accommodative vergence in the alert monkey motor unit analysis. *Vision Res.* 13: 1565–1575, 1973.

KRAUZLIS, R. J. AND LISBERGER, S. G. Simple spike responses of gaze velocity purkinje cells in the floccular lobe of the monkey during the onset and offset of pursuit eye movements. *J. Neurophysiol.* 72: 2045–2050, 1994.

LISBERGER, S. G. The neural basis for learning of simple motor skills. *Science* 242: 728–735, 1988.

LISBERGER, S. G., PAVELKO, T. A., BRONTE-STEWART, H. M., AND STONE, L. S. Neural basis for motor learning in the vestibuloocular reflex of primates. II. Changes in the responses of horizontal gaze velocity Purkinje Cells in the cerebellar flocculus and ventral paraflocculus. *J. Neurophysiol.* 72: 954–973, 1994.

MILES, F. A., FULLER, J. H., BRAITMAN, D. J., AND DOW, B. M. Long-term adaptive changes in primate vestibuloocular reflex. III. Electrophysiological observations in flocculus of normal monkeys. *J. Neurophysiol.* 43: 1437–1476, 1980.

MILES, F. A., KAWANO, K., AND OPTICAN, L. M. Short-latency ocular following responses of monkey. I. Dependence on temporospatial properties of visual input. *J. Neurophysiol.* 56: 1321–1354, 1986.

NEWSOME, W. T., WURTZ, R. H., AND KOMATSU, H. Relation of cortical areas MT and MST to pursuit eye movements. II. Differentiation of retinal from extraretinal inputs. *J. Neurophysiol.* 60: 604–620, 1988.

REINHART, R. J. AND ZUBER, B. L. Horizontal eye movements from abducens nerve stimulation in the cat. *IEEE Trans. Biomed. Eng.* 17: 11–14, 1970.

ROBINSON, D. A. The mechanics of human smooth pursuit eye movement. *J. Physiol. (Lond.)* 180: 569–591, 1965.

SAKATA, H., SHIBUTANI, H., AND KAWANO, K. Functional properties of visual tracking neurons in posterior parietal association cortex of the monkey. *J. Neurophysiol.* 49: 1364–1380, 1983.

SHIDARA, M. AND KAWANO, K. Role of Purkinje cells in the ventral paraflocculus in short-latency ocular following responses. *Exp. Brain Res.* 93: 185–195, 1993.

SHIDARA, M., KAWANO, K., GOMI, H., AND KAWATO, M. Inverse dynamics model eye movement control by Purkinje cells in the cerebellum. *Nature* 365: 50–52, 1993.

STONE, L. S. AND LISBERGER, S. G. Visual responses of Purkinje cells in the cerebellar flocculus during smooth pursuit eye movements in monkeys. I. Simple spikes. *J. Neurophysiol.* 63: 1241–1261, 1990.

TAKEMURA, A., INOUE, Y., GOMI, H., KAWATO, M., SHIDARA, M., AND KAWANO, K. A linear regression time-series analysis of neural activity during ocular following. Proc. SICE *The 9th Symposium on Biological and Physiological Engineering.* 1994, p. 275–278.

ZHANG, Y., PARTSALIS, A. M., AND HIGHSTEIN, S. M. Properties of superior vestibular ncleus flocculus target neurons in the squirrel monkey. I. General properties in comparison with flocculus projecting neurons. *J. Neurophysiol.* 73: 2261–2278, 1995.